JOURNAL OF GUIDANCE, CONTROL, AND DYNAMICS
Vol. 31, No. 4, July–August 2008

Engineering Notes

ENGINEERING NOTES are short manuscripts describing new developments or important results of a preliminary nature. These Notes should not exceed 2500 words (where a figure or table counts as 200 words). Following informal review by the Editors, they may be published within a few months of the date of receipt. Style requirements are the same as for regular contributions (see inside back cover).

Sliding-Mode Control of a Nonlinear Model of an Unmanned Aerial Vehicle

Ronald A. Hess* and Maryam Bakhtiari-Nejad†
University of California, Davis, Davis, California 95616

DOI: 10.2514/1.32558

Introduction

A FLIGHT control design technique based upon sliding-mode control (SMC) as interpreted in the frequency domain has been exercised in a number of recent studies [1–5]. Although the design technique in these studies has resulted in significant robustness to the effects of modeled vehicle damage, the vehicle models themselves have been linear in nature. The goals of the research to be described are the 1) use of a nonlinear vehicle model in computer simulation of the design and 2) comparison of the performance of the resulting design to that of a nonlinear inversion controller that has been described in [6].

Vehicle Model

The ducted-fan vehicle for which the model will be used in the study is shown in Figs. 1 and 2. The diameter of the duct is 29 in. The unmanned aerial vehicle (UAV) has actuator-driven vanes within the duct in the downwash of the vehicle's propeller. The vane sets are deflected collectively or differentially to create moments about each of the body axes with variable engine rpm controlling thrust. The vanes are coupled in the vehicle model and must share control responsibility between axes. Four actuators mounted inside the duct actuate the control vanes. The actuator models are rate- and amplitude-limited. The bandwidth of each actuator was approximately 38 rad/s, with vane amplitude and rate limits of ± 30 deg and ± 100 deg/s, respectively. A simple engine model is included, consisting of a first-order lag with a 0.25-s time constant. A body-fixed helicopter axis system is employed in this study, with the z-body axis directed downward and coincident with the rotor axis.

At hover, the vehicle dynamics exhibit two pairs of unstable eigenvalues: $+1.493 \pm 1.196j$ and $+0.0971 \pm 2j$; at 50 ft/s, the dynamics exhibit three real unstable eigenvalues at $+2.356$, $+1.8874$, and $+0.651$. The dynamics of the vehicle also undergo large variations with airspeed. For example, Table 1 shows variations in the elements of linearized vehicle dynamics ($\dot{\mathbf{x}} = \mathbf{Ax} + \mathbf{Bu}$) between hover and 50-ft/s airspeed.

Presented as Paper 6088 at the Guidance, Navigation, and Control Conference, Keystone, CO, 21–24 August 2006; received 1 June 2007; revision received 13 January 2008; accepted for publication 24 January 2008.

*Professor, Department of Mechanical and Aeronautical Engineering. Associate Fellow AIAA.

†Graduate Student, Department of Mechanical and Aeronautical Engineering.

Sliding-Mode Control

The summary of SMC given here is brief, with emphasis on implementation and design issues. The key properties of a sliding mode can be found in [7]. With one exception (the addition of the eighth step), the discussion in this section closely follows that offered in [4].

1) The vehicle model is obtained. Actuator dynamics are not included in the nominal plant model at this juncture.

2) The desired feedback structure of the control system is determined with a square system architecture. If there are redundant control effectors, a control distribution matrix must be defined.

3) The sliding manifolds for each control channel are selected. Recognizing that a boundary layer is to be implemented, the control law is expressed as a linear transfer function:

$$u(s) = \rho\left(s^{\xi-1} + K_{\xi-2}s^{\xi-2} + \cdots + K_0 + \frac{K_{-1}}{s}\right)e(s) \qquad (1)$$

where ξ is the relative order of the control loop in question. The parameters K_i are chosen to provide desirable properties in the frequency domain. This step is completed without the observer or actuators. Very high crossover frequencies will typically be in evidence here.

4) The existence of a sliding mode is verified (here, through computer simulation).

5) The boundary layer is included in the controller.

6) Parasitic (actuator) dynamics are included in the model. The SMC controller will very likely be unstable at this juncture.

7) An asymptotic observer is created. The observer eigenvalues can be selected as real and identical. The magnitude of these eigenvalues are chosen by creating *effective unity-feedback loop transmissions* $L_{(x)}$ and by choosing the largest eigenvalues that will provide acceptable stability margins in $L_{(x)}$. With observer(s) included, the closed-loop system will now be stable.

8) The observer of step 7 is scheduled with the vehicle flight condition. Typically, this will not require changes in the definitions of the controller designed in steps 3–5.

SMC Design for the 29-Inch UAV

Design Specifics, Inner Loops

The design approach for the SMC system will follow the preceding outlined steps. The SMC approach will be used only for the inner attitude-rate loops.

1) The nonlinear vehicle model of [6] is linearized for the purposes of design. All computer simulations will use the resulting design with the full nonlinear model.

2) The control architecture was created with the structure shown in Fig. 3 Here, the Earth-fixed velocity components U, V, and W are transformed to body-fixed velocity components u, v, and w. These velocities are controlled through vehicle Euler angles, which are in turn controlled through body-axis rates and then through vane angles. Yaw attitude ψ receives no outer-loop command and is controlled through yaw rate r. Finally, the z-body-axis velocity component w is controlled through the engine rpm. Only the variables within the box in Fig. 3 are involved directly with the SMC design.

3) Neglecting actuator dynamics, the relative order of each of the square input/output systems was one. Obtaining the desirable

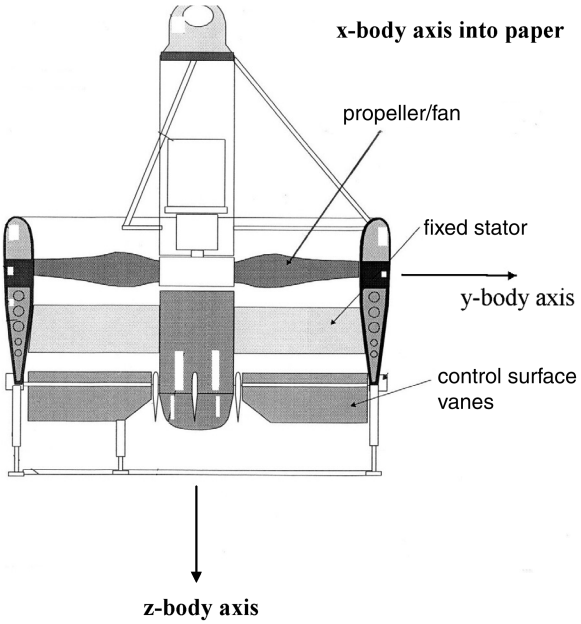

Fig. 1 A schematic diagram of the UAV.

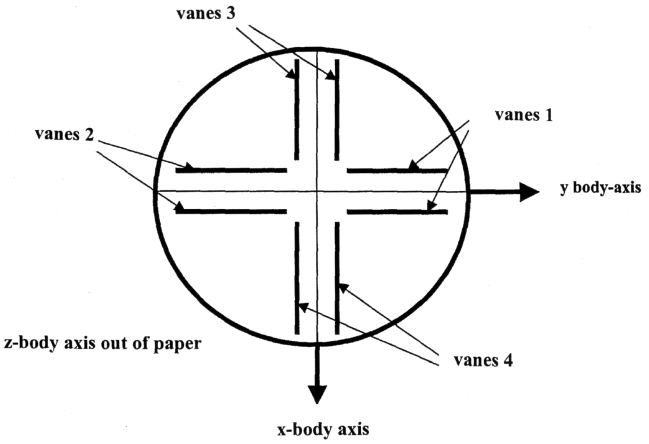

Fig. 2 Vane arrangement for UAV (vehicle viewed from beneath).

K/s-like loop transmissions in each loop led to the following versions of Eq. (1), in which e represents error in the control loop in question:

$$u(s) = \rho\left[1 + \frac{2}{s}\right]e(s) \tag{2}$$

where, for the inner attitude-rate loops,

Table 1 Variation in linear state space matrix elements between hover and 50-ft/s flight conditions

A and B matrix elements	Percent change from hover
A(5,1)	−195 (including sign change)
A(4,2)	+32
A(1,1)	−46
A(1,3)	+988 (including sign change)
A(2,2)	−29
A(3,3)	−94
B(5,1)	+31
B(4,2)	+32
B(6,3)	−10
B(3,1)	−20

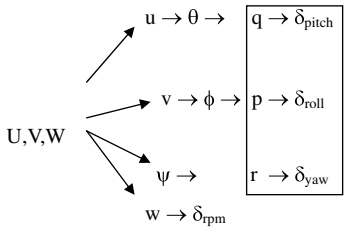

Fig. 3 Control architecture.

$$\rho_q = 90 \qquad \rho_p = 150 \qquad \rho_r = 75 \tag{3}$$

yielded a crossover frequencies of 50 rad/s. The caveat concerning large crossover frequencies mentioned in design step 3 in the previous section is repeated here.

4) Sliding behavior was verified through computer simulation.

5) Boundary layers were included in the controller.

6) As expected, the attitude-rate control systems were unstable when the actuator dynamics were included.

7) A single asymptotic observer was created to service each of the attitude-rate SMC channels. The measured variables were attitude rates p, q, and r; attitudes ϕ, θ, and ψ; and body-axis velocity components u, v, and w. These variables were chosen because they are identical to those used in [6]. The design tradeoff was conducted in the frequency domain by comparison of the Bode plots of *effective* unity-feedback loop transmissions for each control loop in question, with the remaining inner loops closed. For example, for the pitch-rate loop, an effective unity-feedback transfer function can be obtained as

$$L_q = \frac{q/q_c}{1 - (q/q_c)} \tag{4}$$

where q/q_c is the closed-loop transfer function between the pitch rate and pitch-rate command. Eigenvalue selection was based upon a tradeoff between maximizing both low-frequency Bode magnitude and phase margin. Only those response variables required by the SMC system (p, q, r) were obtained from the observer. The resulting crossover frequency for all attitude-rate loops is approximately 20 rad/s. Attitude loops were closed with crossover frequencies of approximately 5.5 rad/s. The outer body-axis velocity loops were closed, with crossover frequencies of approximately 1.1 rad/s. In each case, desirable K/s-like loop transmissions were in evidence around crossover, with crossover frequency ratios between successive loops of approximately 3.6 and 5.

8) The observer was scheduled with the flight condition defined as steady level flight at velocities from 0 (hover) to 50 ft/s in 10-ft/s increments, with linear interpolation of the matrix elements between flight conditions.

Design Specifics, Outer Loops

The compensation for the θ, ϕ, and ψ loops were simple gains given by

$$K_\theta = K_\phi = K_\psi = 4.62 \ 1/\text{s} \tag{5}$$

The compensation for the x, y, and z-body-axis velocity loops (u, v, and w velocity components) were

$$G_u = -G_v = \frac{0.034(s + 0.6)}{s} = 0.034 + \frac{0.0204}{s} \ \text{rad/(ft/s)} \tag{6}$$

$$G_w = \frac{-26.8(s + 3.5)}{s + 20} \ \text{rad/(ft/s)} \tag{7}$$

An outer y Earth-fixed-axis position loop for the task to be described was designed. The compensation for this loop was a pure gain; that is,

$$G_y = 0.111/\text{s} \tag{8}$$

and possessed a crossover frequency of 0.1 rad/s.

Stability Margins

Gain and phase margins for the feedback loops used in the SMC design (attitude-rate loops) for the vehicle at hover and at a constant forward speed of 50 ft/s with the SMC design are given in Table 2. These margins were obtained through a computer simulation of the SMC-controlled vehicle in equilibrium flight at hover and at 50 ft/s using the complete nonlinear vehicle model.

Design Comparison

The fact that a vehicle model identical to that employed here was used in the nonlinear dynamic-inversion control design of [6] now invites a performance comparison. The work of [6] includes gain and phase margins for pitch, roll, and yaw loops when the loops were cut immediately before the actuators. These margins are shown in Table 3. The margins shown in Table 2 for the SMC design are seen to be comparable with those in Table 3.

Computer Simulation Results

The flight task to be simulated consisted of the vehicle starting from a stabilized hover with x and z Earth-fixed-axis inertial velocity commands. The x velocity command reached a 50-ft/s maximum and lasted approximately 50 s. The z velocity command reached a maximum value of approximately 18 ft/s with a shorter duration. The command time histories were chosen to be similar to those used in [6] with the dynamic-inversion controller. The vehicle was subjected to random turbulence with 10-ft/s root-mean-square (rms) values in each of the three Earth-fixed-axis directions. The turbulence signals were created by passing white noise through first-order filters. No wind or turbulence estimation was employed in the system.

Sensor noise was included for each measured variable. Each noise component consisted of white noise passed through a second-order filter with a 10-rad/s break frequency. The rms values for each additive noise were 5 ft for vehicle position, 0.1 ft/s for body-axis velocities, and 0.1 deg/s and 0.1 deg for attitude rates and attitudes, respectively. Vehicle position was used only to provide outer-loop lateral guidance in the simulation to be discussed. To smooth the position signal in question, it was passed through a second-order filter with unity bandwidth. Unmodeled 0.01-s time delays were included in each loop just after the SMC compensators and in each sensor loop. Finally, because the design is most sensitive to overestimation of the vehicle inertial properties, a 25% unmodeled decrease in the principal moments of inertia in the vehicle was included.

Propeller gyroscopic effects were included the simulation (these were omitted in the study of [6]). No redesign of the SMC system was undertaken to accommodate these effects. Rather, the SMC gains of Eqs. (3) were increased by a factor of 2.5. No other changes in the control system were made. This is not an arbitrary change, because one primary means of reducing cross-coupling effects in any control system is increasing crossover frequencies in the respective loop transmissions.

Table 2 Stability margins for the SMC system

	Phase margin, deg	Gain margin, dB
Pitch-rate loop: hover	42	9.0
Roll-rate loop: hover	40	8.6
Yaw-rate loop: hover	48	10
Pitch-rate loop: 50 ft/s	37	8.7
Roll-rate loop: 50 ft/s	34	8.3
Yaw-rate loop: 50 ft/s	44	8.3

Table 3 Stability margins for nonlinear inversion controller of [6]

	Phase margin, deg	Gain margin, dB
Pitch loop	28.5	4.8
Roll loop	38.3	7.1
Yaw loop	45.2	9.1

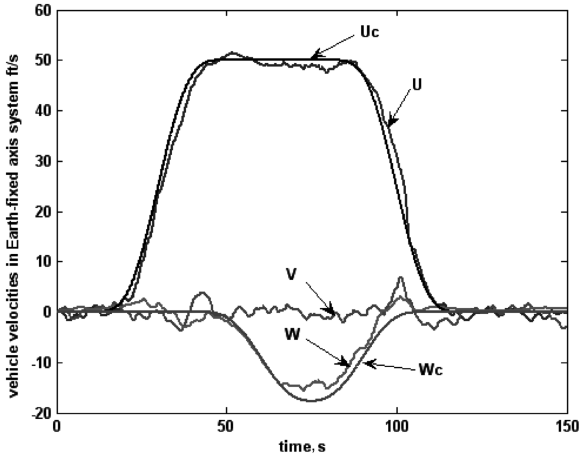

Fig. 4 Vehicle responses; includes propeller gyroscopic effects and 25% unmodeled decrease in principal moments of inertia.

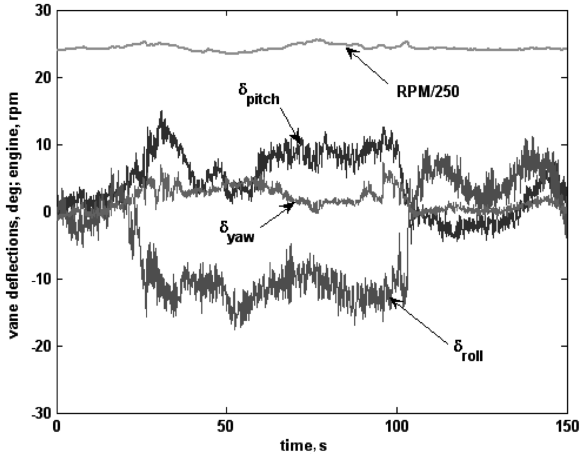

Fig. 5 Vane deflections and rpm for responses of Fig. 4.

Figures 4 shows the tracking performance in the flight condition described. The control input time histories are shown in Fig. 5. The abscissa of Fig. 5 tends to exaggerate the control activity. Figure 6 shows the roll-vane deflection in the time segment $70 < t < 80$ s, with variations between -6 and -13 deg. The largest roll-vane rates in this time segment were ± 50 deg/s, one-half of the rate-saturation limits of the vane actuator.

The three-axis turbulence rms values of 10 ft/s were the largest that could be tolerated with this simulation. As has been pointed out in other studies involving ducted-fan vehicles of this type, sensitivity to winds and turbulence is a major concern [6,8]. The instability is caused by amplitude saturation of the control vanes that must share control responsibility among axes.

If the observers were not scheduled with the flight condition, the previous results held, save that the largest reduction in principal moments of inertia that could be tolerated was 0.86, and an increase in control activity again occurred in the flight segment at the 50-ft/s command velocity. This sensitivity can be minimized by basing the design on the lightest vehicle configuration that is to be flown.

Conclusions

Based upon the research summarized herein, the following conclusions can be drawn:

1) A sliding-mode control system is capable of controlling a model of a nonlinear, unstable, and highly coupled uninhabited air vehicle

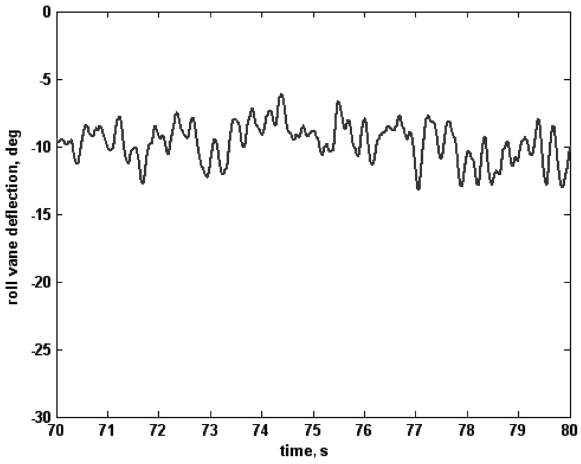

Fig. 6 roll-vane deflection for responses of Fig. 4 for $70 < t < 80$ s.

across a range of flight conditions from hover to 50 ft/s. Significant performance and stability limitations are introduced in the presence of turbulence exceeding approximately 10-ft/s rms values.

2) The sliding-mode design itself can be interpreted as a frequency-domain synthesis technique that creates desirable loop transmissions in sequentially closed control loops.

4) Scheduling the observer used in the sliding-mode design with the flight condition improves the robustness of the system.

5) In a comparison at two flight conditions, the sliding-mode design exhibited stability margins that were comparable with those obtained with a dynamic-inversion design. Comparable performance was also obtained between the sliding-mode and dynamic-inversion controllers when similar flight profiles and disturbance inputs were used in the compute simulations.

6) High-frequency control activity is the price to be paid for the robustness of the sliding-mode design. This activity is adversely affected by sensor noise.

Acknowledgements

The authors are indebted to Christina Spaulding and members of the U.S. Army Aeroflightdynamics Directorate at NASA Ames Research Center for providing the complete nonlinear unmanned aerial vehicle model that was used in this study.

References

[1] Hess, R. A., and Wells, S. R., "Sliding Model Control Applied to Reconfigurable Flight Control Design," *Journal of Guidance, Control, and Dynamics*, Vol. 26, No. 3, 2003, pp. 452–462.

[2] Wells, S. R., and Hess, R. A., "MIMO Sliding Mode Control for a Tailless Fighter Aircraft," *Journal of Guidance, Control, and Dynamics*, Vol. 26, No. 3, 2003, pp. 463–473.

[3] Vetter, T. K., Wells, S. R., and Hess, R. A., "Designing for Damage—Robust Flight Control Design Using Sliding Mode Techniques," *Proceedings of the Institution of Mechanical Engineers, Part G (Journal of Aerospace Engineering)*, Vol. 217, No. 5, 2003, pp. 245–262.

[4] Hess, R. A., and Ussery, T. M., "Frequency-Domain Sliding Mode Design Technique Applied to the Control of a Ducted-Fan Micro-Air Vehicle," *Journal of the American Helicopter Society*, Vol. 49, No. 4, 2004, pp. 457–467.

[5] Hess, R. A., Vetter, T. K., and Wells, S. R., "Design and Evaluation of a Damage-Tolerant Flight Control System," *Journal of Aerospace Engineering*, Vol. 219, No. G4, 2005, pp. 341–360.

[6] Spaulding, C. M., Mansur, M. J., Tischler, M. B., Hess, R. A., and Franklin, J. A., "Nonlinear Inversion Control for a Ducted Fan UAV," AIAA Atmospheric Flight Mechanics Conference and Exhibit, San Francisco, CA, AIAA Paper No. 2005-6231, 5–18 Aug. 2005.

[7] Edwards, C., and Spurgeon, S. K., *Sliding Mode Control*, Taylor and Francis, Bristol, PA, 1998, Chap. 3.

[8] Fleming, J., Jones, T., Gelhausen, P., and Enns, D., "Improving Control System Effectiveness for Ducted Fan VTOL UAVs Operating in Crosswinds," 2nd AIAA Unmanned Unlimited Systems, Technologies, and Operations-Aerospace, San Diego, CA, AIAA Paper No. 2003-6514, 15–18 Sept. 2003.